Physics Letters B 811 (2020) 135951

Contents lists available at ScienceDirect

Physics Letters B

www.elsevier.com/locate/physletb

Low-lying electric dipole γ-continuum for the unstable ^{62,64}Fe nuclei: Strength evolution with neutron number

R. Avigo [a,b], O. Wieland [a,*], A. Bracco [a,b], F. Camera [a,b], F. Ameil [c], T. Arici [c], A. Ataç [d], D. Barrientos [e], D. Bazzacco [f], P. Bednarczyk [h], G. Benzoni [a], B. Birkenbach [i], N. Blasi [a], H.C. Boston [j], S. Bottoni [a,b], S. Brambilla [a], B. Bruyneel [k], M. Ciemała [h], E. Clément [l], M.L. Cortés [m,c], F.C.L. Crespi [a,b], D.M. Cullen [n], D. Curien [o], F. Didierjean [o], C. Domingo-Pardo [q], G. Duchêne [o], J. Eberth [i], A. Görgen [p], A. Gadea [q], J. Gerl [c], N. Goel [c], P. Golubev [r], V. González [q], M. Górska [c], A. Gottardo [f,u], E. Gregor [c], G. Guastalla [m,c], T. Habermann [c], L.J. Harkness-Brennan [j], A. Jungclaus [s], M. Kmiecik [h], I. Kojouharov [c], W. Korten [k], N. Kurz [c], M. Labiche [t], N. Lalović [r], S. Leoni [a,b], M. Lettmann [m], A. Maj [h], R. Menegazzo [f], D. Mengoni [f,g], E. Merchan [c], B. Million [a], A.I. Morales [a,b], D.R. Napoli [u], C. Nociforo [c], J. Nyberg [v], N. Pietralla [m], S. Pietri [c], Zs. Podolyák [w], V.Yu. Ponomarev [m], A. Pullia [a,b], B. Quintana [x], G. Rainovski [y], D. Ralet [c,m], F. Recchia [f,g], M. Reese [m], P. Regan [w], P. Reiter [i], S. Riboldi [a,b], D. Rudolph [r], M.D. Salsac [k], E. Sanchis [z], L.G. Sarmiento [r], H. Schaffner [c], J. Simpson [t], O. Stezowski [aa], J.J. Valiente-Dobón [u], H.J. Wollersheim [c]

[a] *INFN, Sezione di Milano, I-20133 Milano, Italy*
[b] *Dipartimento di Fisica Universita' degli Studi di Milano, I-20133 Milano, Italy*
[c] *GSI Helmholtzzentrum für Schwerionenforschung GmbH, D-64291 Darmstadt, Germany*
[d] *Department of Physics, Royal Institute of Technology KTH, SE-10691 Stockholm, Sweden*
[e] *CERN, CH-1211 Geneva 23, Switzerland*
[f] *INFN, Sezione di Padova, I-35131 Padova, Italy*
[g] *Dipartimento di Fisica ed Astronomia Galileo Galilei Universita' degli Studi di Padova, I-35131 Padova, Italy*
[h] *Institute of Nuclear Physics, Polish Academy of Sciences, 31-342 Krakow, Poland*
[i] *Institut für Kernphysik, Universität zu Köln, D-50937 Köln, Germany*
[j] *Oliver Lodge Laboratory, The University of Liverpool, Liverpool, L69 7ZE, UK*
[k] *IRFU, CEA/DSM, Centre CEA de Saclay, F-91191 Gif-sur-Yvette Cedex, France*
[l] *GANIL, CEA/DSAM and CNRS/IN2P3, BP 55027, F-14076 CAEN Cedex 05, France*
[m] *Institut für Kernphysik, Technische Universität Darmstadt, D-64289 Darmstadt, Germany*
[n] *Nuclear Physics Group, Schuster Laboratory, University of Manchester, Manchester, M13 9PL, UK*
[o] *Université de Strasbourg, CNRS, IPHC UMR 7178, F-67000 Strasbourg, France*
[p] *Department of Physics, University of Oslo, P. O. Box 1048 Blindern, N-0316 Oslo, Norway*
[q] *IFIC, CSIC-Universidad de Valencia, 46980 Paterna, Valencia, Spain*
[r] *Department of Physics, Lund University, SE-22100 Lund, Sweden*
[s] *Instituto de Estructura de la Materia, CSIC, Madrid, E-28006 Madrid, Spain*
[t] *STFC Daresbury Laboratory, Daresbury, Warrington, WA4 4AD, UK*
[u] *INFN, Laboratori Nazionali di Legnaro, Legnaro I-35020, Italy*
[v] *Department of Physics and Astronomy, Uppsala University, SE-75120 Uppsala, Sweden*
[w] *Department of Physics, University of Surrey, Guidford, GU-27XH, UK*
[x] *Laboratorio de Radiaciones Ionizantes, Universidad de Salamanca, E-37008 Salamanca, Spain*
[y] *Faculty of Physics, St. Kliment Ohridski University of Sofia, 1164 Sofia, Bulgaria*
[z] *Department of Electronic, Engineering Universidad de Valencia, E-46100 Valencia, Spain*
[aa] *Université Lyon 1, CNRS/IN2P3, IPN-Lyon, F-69622, Villeurbanne, France*

* Corresponding author.
E-mail address: oliver.wieland@mi.infn.it (O. Wieland).

https://doi.org/10.1016/j.physletb.2020.135951

ARTICLE INFO

Article history:
Received 5 May 2020
Received in revised form 9 November 2020
Accepted 10 November 2020
Available online 16 November 2020
Editor: B. Blank

Keywords:
^{64}Fe
^{62}Fe
Nuclear structure
Dipole excitation around neutron threshold

ABSTRACT

The γ-ray emission from the nuclei ^{62,64}Fe following Coulomb excitation at bombarding energy of 400-440 AMeV was measured with special focus on $E1$ transitions in the energy region 4-8 MeV. The unstable neutron-rich nuclei ^{62,64}Fe were produced at the FAIR-GSI laboratories and selected with the FRS spectrometer. The γ decay was detected with AGATA. From the measured γ-ray spectra the summed $E1$ strength is extracted and compared to microscopic quasi-particle phonon model calculations. The trend of the $E1$ strength with increasing neutron number is found to be fairly well reproduced with calculations that assume a rather complex structure of the 1^- states (three-phonon states) inducing a strong fragmentation of the $E1$ nuclear response below the neutron binding energy.

The interaction of the atomic nucleus with an electromagnetic field is a topic largely investigated both experimentally and theoretically. It provides useful and selective information on the nuclear structure. Among the possible excitation modes the electric dipole ($E1$) type is of particular interest. It is generally dominated by a strong, collective isovector nuclear vibration, the isovector giant dipole resonance (IVGDR) [1,2]. However, the simple dipole oscillation of nucleons giving rise to the IVGDR mode is not the only focus of the investigation. Several studies concentrate on the details of the low-energy part of the electric dipole response, i.e. the so called pygmy resonance [3]. This is because, it provides relevant information, crucial for testing predictions related to the nuclear equation of state (see [4] and [5] and references therein), and additionally supplies inputs for calculations of the r-process nucleosynthesis [6] and astrophysics [7]. The r-process chain for fast neutron capture involves stable Fe isotopes as seed and goes through ^{62}Fe and ^{64}Fe towards the drip-line. But only little is known about their low-lying $E1$ strength, an important ingredient for this process. Model predictions suggest an increase of E1 strength with neutron number and a sizable difference between stable and unstable isotopes (see supplementary material for this manuscript). It is thus important to provide an experimental ground to test theory far from stability also in view of extending the calculations to the uncharted region of even more neutron rich nuclei. In connection with the present situation on the study of the pygmy resonance, it is important to stress that the main effort is concentrated in understanding the nature of the excitation mode. For this purpose, the investigations are moving in two directions: one is the study of selected nuclei with different probes, the so called multi-messenger approach, the other is to select one probe and investigate various isotopes of the same element, with the ambitious goal to reach neutron-rich nuclei far from stability. These concepts, together with many existing results on the pygmy resonance, are discussed in Refs. [1,3,8,9,5].

Concerning the approach grounded on the use of different probes to populate low-lying 1^- states, the existing extensive work concerns mostly stable nuclei [10–15] for which the used reactions are the electromagnetic (γ,γ') and nuclear inelastic scattering of p, α, C and O particles, at energies for which the interaction has a dominant isoscalar component. In all cases, for each given nucleus comparisons were made of the different excitation cross sections. The overarching picture is that up to approximately an excitation energy between 6-7 MeV the pygmy states have a large isoscalar component.

Within the study of the evolution with neutron number of the dipole strength at energies below the neutron binding energy in stable nuclei, the cases of Sn and Xe were measured, as these elements have the longest chains of isotopes. The results for Sn and Xe isotopes show a marked increase of $E1$ strength and of its fragmentation with increasing neutron number (see [16–18] and references therein), which is found to be in rather good agreement with theory [19–22]. Several calculations exist suggesting that the isovector dipole response has a component shifted to low energy with an enhancement below the binding energy, becoming more and more pronounced by going further and further away from stability (see [5] and references therein). It is clear that the way to test this effect is to extend the investigations for the electromagnetic excitation to nuclei produced as radioactive beams. This can only be done by using virtual photons from the Coulomb excitation with a high Z target. Up to now there are only few measurements of the low-lying $E1$ strength in unstable nuclei. They concern the nuclei of ^{20,22}O, ^{26}Ne, ^{68,70}Ni and ^{130,132}Sn [1,15,23–30]. In ^{68}Ni and ^{130,132}Sn nuclei, low-lying $E1$ strength was found above the neutron separation energy at 9-11 MeV. In contrast, in the more recent work on ^{70}Ni [23], it was possible to infer the presence of strength above and also below the particle binding energy, covering the region 6-11 MeV.

The present work concerns the nuclei ^{62,64}Fe. It was motivated by the search of $E1$ strength in nuclei far from stability below the neutron binding energy, an energy region which is particularly interesting for the modeling of the r-process where the $E1$ decay is competing with neutron capture. In addition, this choice was made to study the evolution of the strength over four isotopes since data for the two stable nuclei ^{54,56}Fe obtained with real photons are available.

The experiment was performed in FAIR-GSI laboratories using ^{62,64}Fe beams at 400-440 AMeV impinging on a 1 g/cm^2 thick Au target. At this bombarding energy the cross section for Coulomb excitation is larger than 10 mb in the region of interest. The radioactive ^{62,64}Fe beams were produced by fragmentation of a primary ^{86}Kr beam delivered by the SIS-18 heavy ion synchrotron at 700 and 900 AMeV and focused on a natural 2.5 g/cm^2 thick Be target. The ions of interest were selected and separated in mass and charge with the in flight Fragment Separator (FRS) [31] and transported to the target area. The settings of the FRS were chosen to accept secondary fragments with a magnetic rigidity corresponding to a specific mass-over-charge ratio. This provided a beam cocktail containing ^{62,64}Fe in a large fraction. The different nuclei contained in the secondary beam were identified uniquely, according to their nuclear charge and mass number on an event-by-event basis. In particular, the incoming isotopes of interest were selected using reconstructed identification scatter plots, namely mass over ion charge (AoQ) versus atomic number (Z). The primary beam intensity of ^{86}Kr was between 8×10^8 and 8×10^9 pps, the count rate after the production target and the first stage of selection was between 1 to 5×10^5 pps and the total number of event-by-event traced and registered Fe isotopes up to the outgoing particle and beam identification at the end of the beamline was 1.4×10^5 for ^{64}Fe and 1.8×10^6 for ^{62}Fe. The corresponding identification plots are shown in the top part of Fig. 1, panel a) for ^{62}Fe and panel b) for ^{64}Fe. The two beams of Fe isotopes, ^{62}Fe and ^{64}Fe, are clearly separated from the other isotopes. The outgoing ions,

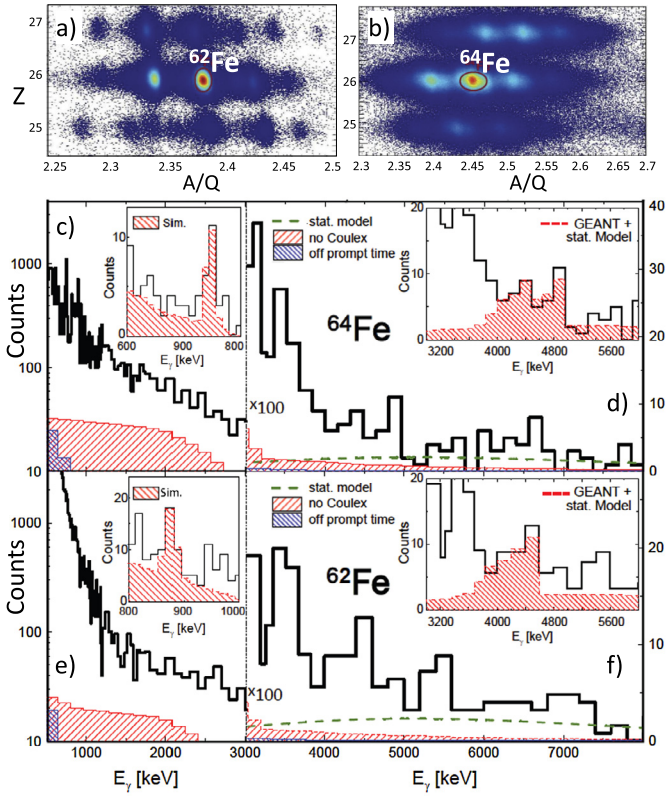

Fig. 1. Top panels a) and b) show the particle identification plots obtained when the fragment separator was set for the optimal transmission of the ^{62}Fe (left) and ^{64}Fe (right) secondary beams. The circles indicate the isotopes of interest. Panels c) to f) show the low energy part (left) and high energy part (right) of the measured γ spectra. The shaded areas in these figures display the spectral shapes obtained with gates corresponding to events outside the Coulomb excitation conditions (red area) or out of the prompt time of flight peak (blue area). The dotted lines (green) in panels d) and f) give the calculated statistical contribution to the spectra. The insets in the panels c) and e) display the known transitions from the first 2^+ states, as obtained with full tracking together with the Monte Carlo simulations of the expected peak. In the insets of panels d) and f) the counts forming peak structures at around 4.5 MeV are compared with simulations taking into account the detection conditions. An increase of the bin size with energy has been chosen to take account for the efficiency loss in the detection of high energy γ rays.

after interaction with the secondary Au target nuclei, were identified and selected using four pieces of information: energy loss, total energy, time of flight and deflection angle. All these quantities were measured with a special calorimetric detector system [32–34], called LYCCA (Lund-York-Cologne CAlorimeter) and placed behind the secondary target covering angles around zero degree and a system of fast scintillators. In the present case, particle multiplicity of one and very small deflection angles of 8 ± 1 mrad, far below the grazing angle, were chosen in order to assure Coulomb excitation to be the main interaction mechanism. This corresponds to values of the impact parameter larger than 17 fm, at which the nuclear contribution of the dipole excitation cross section is strongly suppressed (see [23] and ref. therein).

For the work presented in this paper, the γ rays were measured with AGATA (Advanced GAmma Tracking Array) [35] placed around the Au target. AGATA was installed in the PreSPEC (Pre SPECtroscopy) configuration [32,36–40] and consisted in 5 triple and 3 double clusters of segmented HPGe (High Purity Germanium) detectors mounted in forward angles between 15 to 60 degree (with an add back efficiency of 3% at 1 MeV determined with source calibration runs and validated with GEANT simulations). Energies up to 20 MeV were measured with the segmented HPGe detectors of AGATA which are equipped with digital electronics allowing pulse shape analysis (PSA) of the signals. This leads to a very precise information on the γ ray interaction position ($\sigma \approx 2$ mm), which is crucial if one wants to minimize the Doppler broadening of the measured spectral lines. In addition, the γ-ray tracking allows to increase the peak-to-total ratio in the spectrum [41] and to lower the background. This is especially important at lower energies where a high atomic background is present. For what concerns high energy γ rays, the response of the AGATA was validated in ref. [42].

The γ rays detected with AGATA were measured in coincidence with incident and outgoing ions, whose position information was used to apply the Doppler correction. In this case γ rays were emitted from projectiles moving with a velocity up to 72% of the speed of light. The γ-ray spectra discussed below are all corrected for Doppler shift using the velocity and direction of the scattered beam particles with respect to the first interaction point of the γ ray, which is for energies higher than some hundreds of keV in general the one with the highest deposited energy. In addition to the pulse shape analysis, the add-back technique was used [42]. For the energies up to 1 MeV, the full tracking technique, suited for this energy region, was also exploited in order to better reconstruct the low-energy γ transitions.

The γ rays from the first 2^+ states in ^{62,64}Fe at energy of 0.746 and 0.877 MeV, respectively, are visible. The measured spectra in AGATA are shown up to 3 MeV in Fig. 1 c) and e). The inset in each panel displays the region around the first $2^+ \rightarrow 0^+$ peak for ^{64}Fe the 600-800 keV and for ^{62}Fe the 800-1000 keV region. Since the energy and the $E2$ strength of the 2^+ states of ^{62,64}Fe are well known (see [43] and ref. therein) their $B(E2)$ values were used to calculate the population cross section via distorted wave Born approximation (DWBA) and relativistic coupled-channel (CC) approaches [44,45]. Using a Monte Carlo (GEANT4) code [46,47], the γ-ray interaction distribution inside AGATA was simulated and analyzed with the same procedure employed in the experimental data analysis. An atomic X-ray background at low energies was also included. Peak structures before and after the $2^+ \rightarrow 0^+$ peak of interest were included in the evaluation as background. They do not influence the result as Compton events are strongly suppressed by the very effective tracking. All uncertainties like beam straggling, spreading in the target, detector resolution, dead layers, time and space limitations and losses were included in the simulation made to deduce the measured counts for the first excited state. The obtained intensity of the simulated $2^+ \rightarrow 0^+$ decays of the two ^{62,64}Fe isotopes was found to match the best reported value in the literature only after an additionally correction of 20% (similar to the findings in [48,49]). In this way, the known $B(E2)$ values were used as a reference to extract new information on $E1$ transitions from higher lying states in the same nucleus.

The γ-ray spectra measured at energy larger than 3 MeV are shown in panels d) and f) for the ^{64}Fe and ^{62}Fe nuclei, respectively. The binning was chosen to be consistent with the obtained statistics. This part of the spectra below the neutron threshold and the IVGDR, is the region of interest in which the search for $E1$ transitions, which could originate from 1^- states, is done. The detectors were calibrated in this region with ^{88}Y, PuC and AmBe(Ni) γ-ray sources emitting γ rays of 1.836, 4.438, 6.13 and 9. MeV. The measured spectra shown in Fig. 1 d) and f) have a quasi-continuum feature, with some peak structures in the region 4-6 MeV. Few counts are found up to 7.5 MeV and the statistics is not sufficient to detect γ decay events above the neutron separation energy, which is 7.4 MeV in ^{64}Fe and 8.0 MeV in ^{62}Fe.

To interpret the peak structures in terms of the detection features, Monte Carlo simulations were made to be compared with the spectral shape. This comparison is shown in the insets in Fig. 1 d) and f) for calculated peaks with centroids at 4.4 and 5 MeV for ^{64}Fe and at 4.5 MeV for ^{62}Fe, all with a width of $\approx$200 keV. The simulation includes Doppler broadening, target energy broad-

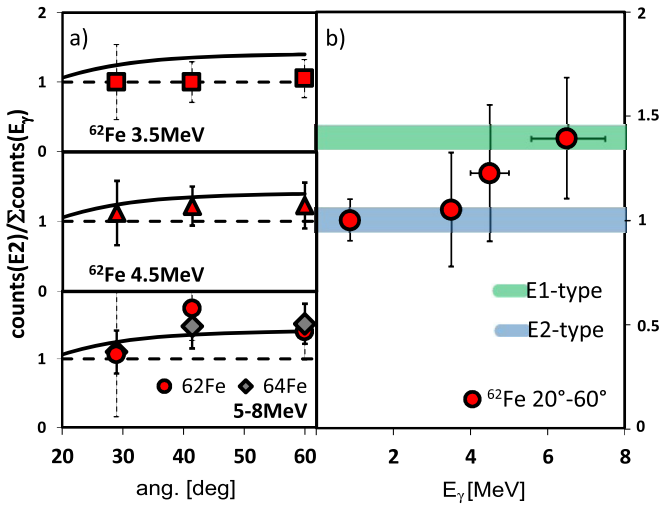

Fig. 2. Panel a): ratio of γ-ray yield in different γ-ray energy regions for ^{62,64}Fe with that of the corresponding 2^+-state as a function of the corresponding angle. The lines give the predictions of the angular distribution for the same ratio assuming pure $E2$ (dashed line) and $E1$ (solid line) transitions. Panel b): the same ratio integrated in angle up to 60 degree as a function of energy. The lines are the predictions for transitions of $E1$ and $E2$ types.

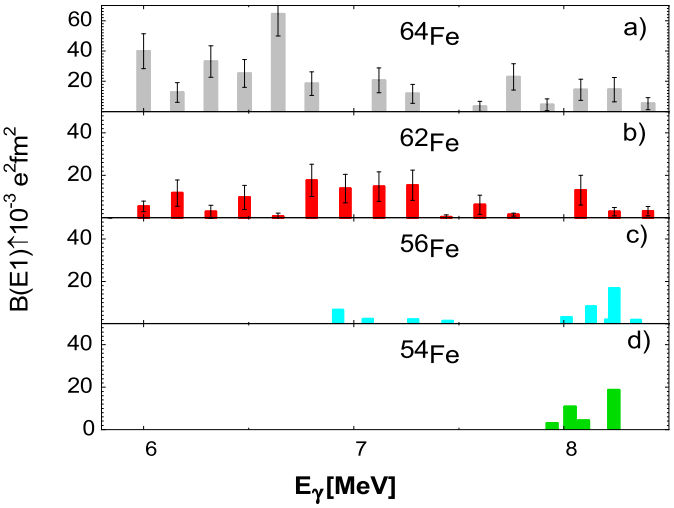

Fig. 3. $B(E1)\uparrow$ strength in the unstable neutron-rich nuclei ^{64}Fe and ^{62}Fe (panel a) and b)) and for the stable nuclei of ^{56}Fe and ^{54}Fe (panel c) and d)) [52,53].

ening and straggling of the impinging beam and uncertainty in the direction of the emitting nucleus, plus the PSA uncertainty in the reconstruction of the interaction points of the γ rays. The yields of events outside the Coulomb excitation angular window and of time uncorrelated events (10 ns out of the prompt time peak) were measured simultaneously and properly normalized to the incoming beam statistics. These distributions are shown with the wide red shaded area and blue narrow shaded area, respectively. The detector response corrected contribution from statistical decay, assuming the standard Lorentzian as a tail of the IVGDR in the projectile, summed to cosmic background events [23,24] is shown with the green dashed line in the high energy spectra of Fig. 1 d) and f). The comparison with the measured spectrum possibly shows a difference in size and shape indicating that the $E1$ strength is different in this case from the tail of a Lorentzian shape for the IVGDR systematics. We note that for the present configuration of AGATA the statistical decay from the target when corrected for the Doppler shift of the projectile, produces counts in the region below 2 MeV and thus can be very well decoupled from the projectile emission which is the focus of this experiment.

At this bombarding energy, in the excitation region larger than 5 MeV the Coulomb excitation mechanism is dominated by exchange of virtual photons of $E1$ type. To verify this relevant point, the angular distributions of counts were measured for different energy regions of the γ-ray spectra. The difference in the angular distribution between $E1$ and $E2$ type due to the effect of the Lorentz boost is very small and far below the detection capabilities, but the ratio between them is detectable. For this reason, the angular distributions of γ transitions from the first 2^+ states were used as reference. Fig. 2 a) shows the ratio of γ-ray yields of ^{62,64}Fe with the ones of the corresponding 2^+-state decay, for energies at 3.5 MeV, 4.5 MeV and above 5 MeV. The data are compared with the corresponding predictions. In Fig. 2 b) the data for ^{62}Fe are shown as a function of γ-ray energy and from there one sees that γ transitions above 5 MeV have $E1$ character. Therefore the continuum type spectrum above 5 MeV is the one for which the discussion in connection with theory is considered, for further analysis and interpretation. In particular, $B(E1)$ strengths were obtained in this quasi-continuum region where the $E1$ character dominates. The measured spectra were converted directly into $E1$ strength considering the detector efficiency and a bin size of 160 keV. The counts were background subtracted. The background consisted in off prompt, no Coulomb excitation events, as shown in Fig. 1, and in a continuum cosmic event background which was measured during and after the experiment for events with energy higher than 20 MeV. The total background contribution amounted to about 1 count per bin in the present configuration. The measured counts in the high energy continuum region were then corrected for the detection efficiency and response function. After subtracting the background, the counts were converted into cross section. The conversion into B(E1) strength used the method of the relativistic Coulomb excitation of Ref. [50,51,23] and assumed virtual photons of E1 type in the region above 6 MeV. In doing this the energy variation of the virtual photon yield was taken into account. We note that no valuable feeding to lower states was found in γ-γ coincidence spectra and no isomers were detected in the off prompt or in the beam like implantation spectra. The corresponding $E1$ strength values in the region above 6 MeV are shown in Fig. 3 in the two top panels, for ^{64}Fe and ^{62}Fe. The error is approximately 35%. The integrated $E1$ strength between 6 and 8 MeV is 0.26 ± 0.10 and 0.10 ± 0.03 e^2 fm^2 for ^{64}Fe and ^{62}Fe, respectively.

The measured spectra from which the $E1$ strength was obtained are dominated by a continuum structure due to the experimental conditions, and data are restricted to observable energy region up to $\approx$8 MeV. The main finding is an increase with neutron number of the total $E1$ strength and of its fragmentation, which shifts the strength towards lower energy.

The experimental results are compared with the $B(E1)$ values reported in the literature for ^{54}Fe and ^{56}Fe isotopes resulting from γ scattering experiments [52,53], they are displayed in the two bottom panels of Fig. 3. One can see an increase of the $E1$ strength with the neutron excess and the shifting down of strength to lower energy in the case of the more neutron-rich isotopes of ^{62}Fe and ^{64}Fe. In addition, there is a noticeable increase of the strength in ^{64}Fe nucleus with respect to the one in ^{62}Fe, due to the addition of only two neutrons. A neutron effect is thus visible in the $E1$ strength below the neutron separation energy. In particular, the summed $E1$ strength is shown in panel a) of Fig. 4. In ^{64}Fe, it is found to be approximately 2 to 4 times larger than that in ^{62}Fe. The spectra of the theoretical calculations (discussed below) are also shown. They have been binned in a way to be comparable to the experimental findings (the unbinned theoretical data can be found in the supplementary materials to this manuscript).

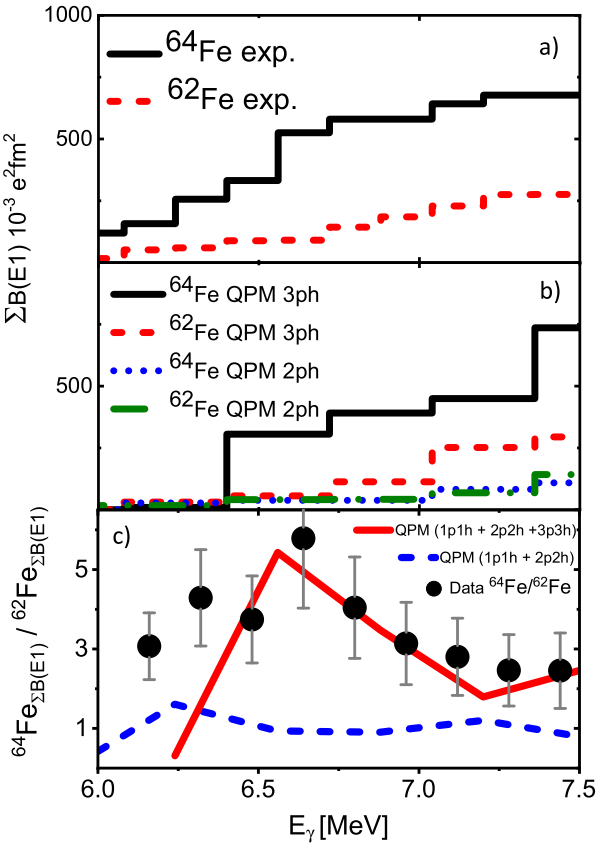

Fig. 4. The summed $E1$ strength values, as a function of energy, for data and calculations. Panel a) shows the data for ^{64}Fe with solid line and for ^{62}Fe with dashed line. In panel b) the binned QPM calculations are shown: for the 3-phonon model (3ph) for ^{64}Fe (full line) and for ^{62}Fe (dashed line) and for the 2-phonon model (2ph) for ^{64}Fe (dotted line) and for ^{62}Fe (dash-dotted line). Panel c) shows the ratio of the summed strength for data and calculations for the two nuclei ^{64}Fe and ^{62}Fe. The dashed curve corresponds to a calculation in which only 2p-2h states are included.

To describe the obtained results calculations were made for the ^{62,64}Fe isotopes in the framework of the quasi-particle phonon model (QPM) [54]. This model has been widely used from the late 90's [55,56] to describe the extensive existing data of pygmy states from (γ, γ') experiments. The QPM predictions are well suited to describe the $E1$ strength at low energy among the many available predictions of the dipole response (see, e.g. [3] for review). This is because the model considers complex configurations by going beyond the simple one-particle one-hole (1p-1h) states and including two-particle two-hole (2p-2h) or even three-particle three-hole (3p-3h) configurations. In particular, the QPM uses single-particle energies from a global Woods-Saxon parametrization obtained from a fit to experimental data over a wide mass range [57]. The simplest modes of nuclear excitation are treated as phonons (ph) which are obtained by solving quasiparticle RPA equations on 1p-1h basis. The excited levels are assumed to have more complex structure: their wave functions contain a mixture of 1ph and 2ph (and 3ph) components. The former plays a role of doorway states and carry the major part of the excitation $E1$ strength. The latter are the background configurations, their density increases exponentially with excitation energy and they participate in fragmentation of the strength of the doorway components. Following this approach the QPM calculations are found to give a rather realistic description and a rather good account of the strongly fragmented experimental strength seen in many stable neutron rich nuclei in different nuclear reactions [58]. Therefore, the description of the present data focuses on the comparison with the QPM predictions.

The $E1$ strength distribution, calculated in the QPM, depends on the strength parameter of the isovector residual interaction and is shown and explained in Fig. 4 in the Supplementary Material. In Fig. 4 the QPM predictions for the summed $E1$ strength in ^{62}Fe and ^{64}Fe are shown in panel (b), while the corresponding experimental data are shown in panel a). One sees that the calculations follow well the experimental trend. In addition, the relative increase is also reasonably accounted. Indeed, the summed $E1$ strength in ^{64}Fe is found to be approximately 2 to 4 times larger than that in ^{62}Fe in the observed energy range, similarly to the experimental data. In order to emphasize this relative increase of the summed $E1$ strength as a function of energy the ratio of the strength in the two isotopes is shown both for the data and the calculations in panel (c). An additional prediction (dashed line) is also shown and this considers only up to 2ph configurations. This last calculation is far away from the experimental data and predicts a rather small variation of strength among the two isotopes. We notice that the lowest 1ph configurations in both ^{62,64}Fe isotopes have excitation energy of about 9 MeV and their $B(E1)$ values are too small in comparison to data (see Fig. 1 in Supplementary material). In the case of inclusion of 2ph only, a comparable behavior to the observed $E1$ strength appears in this doorway picture only around 11 MeV and it is not much different between the two isotops. Only the coupling of the doorway states to more complex configurations pushes a part of the dipole strength to lower energies and dramatically improves the agreement with data. The coupling is stronger in a softer ^{64}Fe with more collective low-lying phonons, leading to the enhancement of the $E1$-strength below the threshold, in comparison to ^{62}Fe. Otherwise, at higher excitation energies, including the GDR the QPM predicts no essential differences in the $E1$-strength distribution between the two isotopes (see Fig. 1 in Supplementary material). In the supplementary material to this manuscript the strength distribution in 1 phonon approximation is shown for ^{62,64}Fe isotopes in Fig. 1 in Supplementary material, for the 1+2 and 1+2+3 phonon approximation in stable ^{54,56}Fe and unstable ^{62,64}Fe isotopes in Figs. 2 and 3 in Supplementary material. One can note that the low-lying strength for the stable isotopes is one to two orders of magnitude smaller than the exotic ones. The stable isotopes show an even more pronounced effect of increase of strength with neutron number below neutron threshold energy, which opened the question if this trend is still valid for unstable nuclei or damped. The 1 phonon approximation does not show any low-lying states, the two phonon approximation does show little difference in the strength sum between ^{62}Fe and ^{64}Fe. Only the three phonon approximation can reproduce the experimental findings in this manuscript.

The finding of this work, that in the interval 6-7.5 MeV, the summed $E1$ strength is in ^{64}Fe a factor of 2 to 4 times larger than in ^{62}Fe is interesting and this trend is on the other hand in line with what found in stable neutron rich-nuclei [8]. However, the identification of $E1$ strength below binding energy in unstable nuclei is very relevant to test nuclear structure far from stability and how well the models, in this case the QPM, can also describe these nuclei precursors of stable nuclei in explosive nucleosynthesis processes.

In summary, we have measured for the first time $E1$ transitions in the region above 5 MeV up to the neutron separation energy, for the two unstable nuclei ^{62}Fe and ^{64}Fe. These nuclei appear to have a continuum structure in spectra measured with the technique of virtual photon scattering, the only one which allows to access this excitation energy region and populate mostly 1^- states. The comparison with QPM model predictions is made for the summed $E1$ strength as a function of energy. The trends and the relative increase going from the ^{62}Fe nucleus to the ^{64}Fe nucleus are reproduced rather well by the QPM predictions including complex configuration of 1^- states up to 3p3h states. In

contrast, the inclusion of only 2p2h states cannot explain the data. The present findings shed more light on the understanding of the structure of the low-lying $E1$ strength, which is found in the energy region below the particle binding energy to be sizable and to increase with neutron number. Moreover, the fact that the main features for the two measured unstable isotopes are rather well reproduced by the QPM calculations including couplings up to the three particle level, gives a relevant test to this model, which so far was widely used for stable nuclei. However, the description of nuclei even more neutron rich might be more complex as more couplings might be required. The ambition for the future is to go further away from stability with this type of investigations which need also more statistics. With a more efficient AGATA detector, as it is planed to be in the future, and more intense fragmentation beams, this challenging program is expected to be feasible for example within the HISPEC project [59].

Declaration of competing interest

The authors declare that they have no known competing financial interests or personal relationships that could have appeared to influence the work reported in this paper.

Acknowledgements

The authors would like to thank D. Peña Arteaga, X. Roca-Maza for fruitful discussions. The authors would especially thank the FRS team of GSI/FAIR for their work. This work was partially supported by INFN (Italy) and STFC (UK), the Swedish Research Council (Vetenskapsrådet, VR 2010-147, 2011-5253, and 2016-3969), BMBF NuSTAR-AGATA 05P18RDFN9 and BMBF NuSTAR 05P18RDFN1. The project was co-funded by the European Commission under the 7th Framework Program for RTD (2007-2013) under the Capacities Program (Contract Number 262010, ENSAR). This work was partially supported by the Ministry of Science, and Generalitat Valenciana, Spain, under the Grants SEV-2014-0398, FPA2017-84756-C4, PROMETEO/2019/005 and by the EU FEDER funds.

Appendix A. Supplementary material

Supplementary material related to this article can be found online at https://doi.org/10.1016/j.physletb.2020.135951.

References

[1] A. Bracco, et al., Eur. Phys. J. A 55 (2019) 233.
[2] M.N. Harakeh, A. van der Woude, Giant Resonances, Clarendon Press, Oxford, 2002.
[3] A. Bracco, E.G. Lanza, A. Tamii, Prog. Part. Nucl. Phys. 106 (2019) 360.
[4] A. Carbone, et al., Phys. Rev. C 81 (2010) 041301(R).
[5] X. Roca-Maza, N. Paar, Prog. Part. Nucl. Phys. 101 (2018) 96.
[6] S. Goriely, et al., Nucl. Phys. A 739 (2004) 331.
[7] T. Aumann, C. Bertulani, Prog. Part. Nucl. Phys. 112 (2020) 103753.
[8] D. Savran, et al., Prog. Part. Nucl. Phys. 70 (2013) 210.
[9] A. Spyrou, et al., J. Phys. G 44 (4) (2017) 0440022.
[10] F.C.L. Crespi, et al., Phys. Rev. Lett. 113 (2014) 012501.
[11] L. Pellegri, et al., Phys. Lett. B 9738 (2014) 519.
[12] M. Krzysiek, et al., Phys. Rev. C 93 (2016) 044330.
[13] D. Savran, et al., Phys. Rev. Lett. 97 (2006) 172502.
[14] J. Endres, et al., Phys. Rev. C 80 (2009) 034302.
[15] N. Nakatsuka, et al., Phys. Lett. B 768 (2017) 387.
[16] R. Massarczyk, et al., Phys. Rev. Lett. 112 (2014) 072501.
[17] M. Müscher, et al., Phys. Rev. C 102 (2020) 014317.
[18] P. Adrich, et al., Phys. Rev. Lett. 95 (2005) 132501.
[19] E. Litvinova, et al., Phys. Rev. Lett. 105 (2010) 022502.
[20] E. Litvinova, et al., Phys. Rev. C 88 (2013) 044320.
[21] X. Roca-Maza, et al., Phys. Rev. C 88 (2013) 024316.
[22] J. Piekarewicz, Phys. Rev. C 83 (2011) 034319.
[23] O. Wieland, et al., Phys. Rev. C 98 (2018) 064313.
[24] O. Wieland, et al., Phys. Rev. Lett. 102 (9) (2009) 092502.
[25] E. Tryggestad, et al., Phys. Lett. B 541 (2002) 52.
[26] A. Leistenschneider, et al., Phys. Rev. Lett. 86 (2001) 5442.
[27] D. Rossi, et al., Phys. Rev. Lett. 111 (2013) 243503.
[28] J. Gibelin, et al., Phys. Rev. Lett. 101 (2008) 212503.
[29] P. Adrich, et al., Phys. Rev. Lett. 95 (2005) 132501.
[30] N. Martorana, et al., Phys. Lett. B 782 (2018) 112.
[31] H. Geissel, et al., Nucl. Instrum. Methods Phys. Res. B 70 (1992) 286.
[32] N. Pietralla, et al., Eur. Phys. J. Web Conf. 66 (2014) 02083.
[33] P. Golubev, et al., Nucl. Instrum. Methods Phys. Res., Sect. A 723 (2013) 55.
[34] R. Hoischen, et al., Nucl. Instrum. Methods Phys. Res., Sect. A 654 (2011) 354.
[35] S. Akkoyuna, et al., Nucl. Instrum. Methods Phys. Res., Sect. A 668 (2012) 26.
[36] D. Ralet, et al., Nucl. Instrum. Methods Phys. Res., Sect. A 786 (2015) 32.
[37] D. Ralet, et al., Phys. Rev. C 95 (2017) 034320.
[38] N. Lalović, et al., Nucl. Instrum. Methods Phys. Res., Sect. A 806 (2016) 258.
[39] C. Domingo-Pardo, et al., Nucl. Instrum. Methods Phys. Res., Sect. A 694 (2012) 297.
[40] A. Korichi, et al., Nucl. Instrum. Methods Phys. Res., Sect. A 872 (2017) 80.
[41] O. Wieland, et al., J. Phys. Conf. Ser. 580 (2015) 012058.
[42] F.C.L. Crespi, et al., Nucl. Instrum. Methods Phys. Res. A 705 (2013) 47.
[43] B. Pritychenko, et al., At. Data Nucl. Data Tables 107 (2016) 1.
[44] J. Raynal, Phys. Rev. C 23 (1981) 2571.
[45] I. Thompson, Comput. Phys. Rep. 7 (1988) 167.
[46] S. Agostinelli, et al., Nucl. Instrum. Methods Phys. Res., Sect. A 506 (2003) 250.
[47] E. Farnea, et al., Nucl. Instrum. Methods Phys. Res., Sect. A 621 (2010) 331.
[48] P. Napiralla, et al., Eur. Phys. J. A 56 (2020) 147.
[49] M. Reese, Ph.D. thesis, TU Darmstadt, 2018.
[50] A. Winther, K. Alder, Nucl. Phys. A 319 (1979) 518.
[51] C. Bertulani, G. Baur, Nucl. Phys. A 458 (1986) 725.
[52] F. Bauwens, Phys. Rev. C 62 (2000) 024302.
[53] E. McCutchan, https://www.nndc.bnl.gov/ensdf/, 2019.
[54] V. Soloviev, Theory of Atomic Nuclei: Quasiparticles and Phonons, Institute of Physics, Bristol, 1992.
[55] R.-D. Herzberg, et al., Phys. Rev. Lett. B 390 (1997) 49.
[56] K. Govaert, et al., Phys. Rev. C 57 (1998) 2229.
[57] V.Y. Ponomarev, et al., Nucl. Phys. A 323 (1979) 446.
[58] D. Savran, et al., Phys. Rev. Lett. B 786 (2018) 16.
[59] Z. Podolyák, Int. J. Mod. Phys. E 15 (2006) 1967.